Processing and Application of Ceramics 13 [4] (2019) 387–400
https://doi.org/10.2298/PAC1904387S

Giant dielectric response in microwave processed $CaCu_3Ti_4O_{12}$ ceramics: A correlation among microstructure, dielectric and impedance properties

Buddhadev Samanta, Dipika Nanda, Pawan Kumar*, Rashmirekha Sahu, Sujata Swain, Apurba Mahapatra

Department of Physics & Astronomy, National Institute of Technology, Rourkela, Odisha, 769008, India

Received 7 January 2019; Received in revised form 9 May 2019; Received in revised form 4 September 2019; Accepted 20 November 2019

Abstract

Polycrystalline $CaCu_3Ti_4O_{12}$ (CCTO) ceramics was synthesized by microwave assisted solid-state reaction. Effect of sintering at different temperatures on the crystal structure, dielectric and impedance properties was investigated in detail. Rietveld analysis of X-ray diffraction data identified that crystal structure was a mixture of cubic CCTO and monoclinic CuO phases. Lattice parameters and amount of CuO secondary phase were also estimated as a function of sintering temperature. Microstructural investigation confirmed the existance and successive increase of the melted phase near the grain boundary region with increasing temperature of sintering. Cu-rich nature of the melted phase was further confirmed by selective area EDX spectra. Dielectric and impedance properties were studied as a function of frequency (100 Hz to 1 MHz) and temperature (room temperature to 300 °C). Improvement in dielectric properties as a function of sintering temperature (1000 to 1050 °C) was explained in terms of reduction in grain boundary dimension due to the successive increase in Cu-rich melted phase. However, dielectric constant started falling when sintered at 1075 °C, which may be accounted in terms of segregation of large amount of CuO phase after a certain temperature and hence a non-stoichiometry of Cu in CCTO lattice. Impedance data were modelled by equivalent electrical circuits to investigate different contributions of electrically heterogeneous systems. In addition, probable relaxation mechanism has been discussed on the basis of impedance and modulus data. Activation energies were calculated from different characterizations and a non-Debye-type relaxation phenomena were observed. In this work, an attempt is made to build up a correlation among synthesis procedure, sintering temperature, dielectric, impedance and microstructural properties.

Keywords: *$CaCu_3Ti_4O_{12}$, microwave processing, structure, dielectric properties, impedance spectroscopy*

I. Introduction

$CaCu_3Ti_4O_{12}$ (CCTO) shows an unusual variation of perovskite structure. Having pseudo perovskite crystal structure, CCTO has attracted considerable considerable interest due to its colossal dielectric permittivity at room temperature ($\approx 10^4$–10^6), which remains almost constant over a wide temperature and frequency range [1–4]. Practical applications of CCTO based systems can enhance the performance and miniaturization of microelectronic devices by virtue of its excellent dielectric properties. Crystal structure of $CaCu_3Ti_4O_{12}$ (CCTO) is cubic (space group $Im\bar{3}$) with centro-symmetry, hence non-ferroelectric in nature [3]. Though, origin of such giant permittivity in this material was anticipated as extrinsic in nature [5,6], it is still ambiguous. In polycrystalline CCTO ceramics, possible and widely accepted extrinsic mechanism is internal barrier layer capacitor (IBLC) model, which is associated with: i) semiconducting or conducting grains (G) and ii) insulating grain boundaries (GB) [7–11]. Sample-electrode interfaces may also contribute to giant permittivity in ceramics which has been previously reported by Lunkenheimer *et al.* [12] as a surface barrier layer structure (SBLC).

*Corresponding authors: tel: +9106612462726,
e-mail: *pvn772004@yahoo.co.in*

Microwave processing of ceramics is very attractive technique for material synthesis because of its advantages like very fast heating, increased densification, decreased sintering activation energy, improved microstructure, selective heating, non-contact heating, grain growth inhibition, energy and cost savings compared to conventional processing of electroceramics etc. [1].

A ceramic disk capacitor consists of a pair of parallel metal plates separated by a dielectric medium [13]. Capacitors are most essential component of electronic circuits and used for electrical energy storage, filtering out electronic noise, high-frequency tuning and so many other potential applications [14]. Among the non-destructive material characterizations, complex impedance spectroscopy (CIS) has been frequently used to probe into microscopic level and explore the different mechanisms behind the dielectric and electrical properties of materials. In polycrystalline ceramics, electrical responses usually arise from: i) grain or bulk, ii) grain boundary and iii) sample electrode interface [2,15]. For the sake of simplicity, each response can be considered as a parallel combination of *R* (resistance) and *C* (capacitance). As a whole, one can think of three parallel *R-C* circuits connected in series. In the Cole-Cole impedance plot, each parallel *R-C* circuit corresponds to semicircular arc having centre on the real impedance (Z') axis for single relaxation time [2]. High frequency arc corresponds to grain and successive arcs towards lower frequency region represent the contribution of grain boundary and sample-electrode interface, respectively. Otherwise, depressed circular arcs having centres below the real impedance axis are associated with distribution of the relaxation time. Constant phase element (Q) is useful to explain non-ideal capacitance in equivalent circuit model and its presence can be attributed to non-ideal bulk relaxations in electroceramics [16,17]. Such equivalent electrical circuit models allow us to discriminate and separate the response of grain (bulk), grain boundary and sample-electrode interfaces by theoretical fitting to experimental data.

In the present work, an attempt has been made to investigate and link the dielectric impedance and microstructural properties of $CaCu_3Ti_4O_{12}$ (CCTO) ceramics, prepared by microwave assisted solid state reaction. Dielectric, impedance and modulus spectroscopic properties were studied as a function of temperature and frequency. Equivalent circuit models were proposed to understand the dielectric properties theoretically and to deconvolute the different contribution of impedance data. A try to establish correlation among synthesis procedure, sintering temperature, dielectric, impedance and microstructural properties has been made in this work.

II. Experimental

Polycrystalline CCTO ceramics was synthesized by microwave assisted solid state reaction using oxide and carbonate precursors. Stoichiometric proportion of $CaCO_3$ (99%), CuO (99%) and TiO_2 (99%) powders was ground in acetone medium for 24 h using zirconium balls to achieve homogeneous mixture. After drying, powder mixture was calcined at 850 °C for 15 min in a microwave furnace (VB Ceramics Hybrid Microwave furnace 2.45 GHZ, with IR temperature sensor) using heating rate of 20 °C/min and cooling rate of 10 °C/min in the presence of susceptor. After adding binder (3% PVA solution), the calcined powder was compacted into green pellets using uniaxial hydraulic press. Finally, the green pellets were sintered at four different temperatures (1000, 1025, 1050 and 1075 °C) for 30 min using heating rate of 25 °C/min and cooling rate of 10 °C/min in the presence of susceptor. We used silver paint (Sigma Aldrich) to create metallic electrode on top surfaces of the sintered pellets fired in a muffle furnace at 450 °C for 30 min to achieve good electrode adhesion. DC gold sputtering was used for surface coating to avoid electron accumulation during FESEM study. This whole synthesis procedure was also reported in our previous work [1]. Abbreviations used for the samples are CCTO1, CCTO2, CCTO3 and CCTO4 in accordance with successive increase in the sintering temperature (from 1000 to 1075 °C).

Co-K_α (λ = 1.789010 Å) radiation (Bruker D8) was used for X-ray diffraction study. Structural refinement was carried out by Rietveld analysis using cubic CCTO with monoclinic CuO secondary phase, which was reported earlier [1]. Dielectric properties were previously studied [1] as a function of frequency (100 Hz to 1 MHz) and temperature (room temperature to 150 °C). In this present work, temperature dependance of dielectric properties was studied within the temperature range from room temperature to 300 °C at four discrete frequencies (1, 10, 100 and 1000 kHz) using LCR meter (Hioki 3532-50, Japan). Impedance data were taken as a function of frequency (100 Hz to 1 MHz) and temperature (room temperature to 300 °C) by an impedance analyser Hioki IM3570, Japan. Surface morphology was studied using FESEM (Nova Nano-SEM) along with EDX spectra taken in the secondary electron mode.

We took kerosene oil as an immersion liquid and measured bulk density of the sintered pellets by the Archimedes principle using the formula:

$$\rho = \rho_k \frac{W_{dry}}{W_{soak} - W_{sus}} \tag{1}$$

where ρ_k = 0.81 g/cm^3 is density of kerosene oil, W_{dry} is dry weight, W_{sus} is suspended weight and W_{soak} is soak weight.

III. Results and discussion

3.1. X-ray diffraction study

Phase purity as well as crystal structure of the sintered pellets were investigated using X-ray diffractometer (Fig. 1). All sintered pellets show diffraction pat-

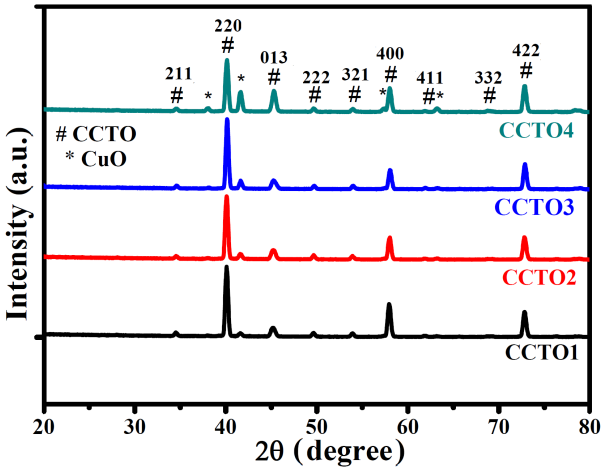

Figure 1. X-ray diffraction patterns of sintered samples

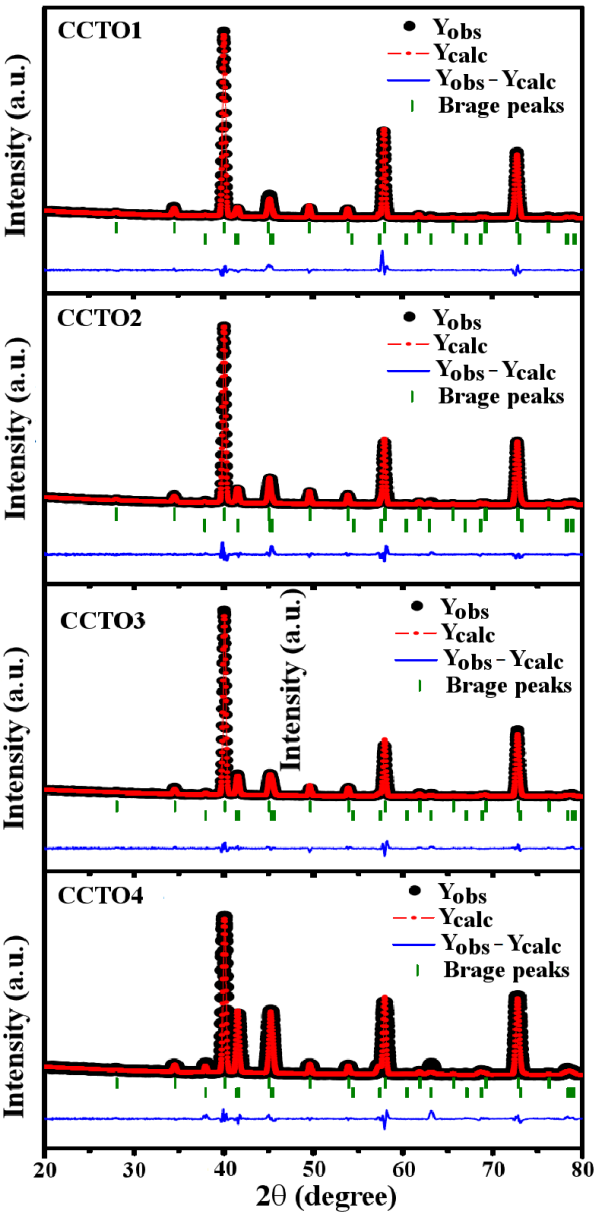

Figure 2. X-ray diffraction pattern of sintered samples refined using Rietveld analysis

tern of the cubic perovskite CCTO phase with space group $Im\bar{3}$ (JCPDS 75-2188) along with several peaks of the secondary phase identified as CuO with monoclinic structure with space group: $C2/c$ (JCPDS 41-0254). Relative intensity of the XRD peak at $2\theta \sim 41.6°$ tends to increase with increasing sintering temperature, which suggests the raise in CuO phase content. Rietveld refinement of the X-ray diffraction data was used to estimate the amount of CuO secondary phase in the sintered CCTO1, CCTO2, CCTO3 and CCTO4 pellets (Fig. 2), which was 6.38%, 10.73%, 15.93% and 34.58%, respectively. Rietveld refinement was also used to obtain crystallographic information like lattice constants, Wyckoff positions etc. Incorporation of such crystallographic information in VESTA software (version 3) enables us to visualize the unit cells with different atoms and their coordination. Figures 3a and 3b graphically demonstrate cubic unit cell of CCTO3 samples with TiO_6 octahedra and square planar configuration of Cu and O atoms, respectively. Figure 3c shows the refined monoclinic unit cell of CuO secondary phase.

3.2. Microstructure

Densities of the sintered CCTO1, CCTO2, CCTO3 and CCTO4 pellets are 4.59, 4.60, 4.64 and 4.61 g/cm^3, respectively. Thus, density of the sintered pellets increased as sintering temperature increased from 1000 to 1050 °C. The pellet CCTO4, sintered at 1075 °C, exhibited lower density compared to the sample sintered at 1050 °C, but still larger than the pellets sintered at 1000 and 1025 °C. The reduction of density for the CCTO4 sample may be due to the volatile nature of Cu.

Figure 4 shows FESEM micrograph of different samples. Inter-granular melt-like phase appeared along with distinct grains in all samples. The amount of melted phase increased with sintering temperature. Non-uniform grain size was observed with accumulation of melted phase mainly near the grain boundary region. Selective area EDX was performed to estimate the individual elemental concentration present in the distinct grains and melted phase (Table 1). Large amount of copper has been found in the melted phase and the stoichiometry of grains and melted phase is completely different. Existence and successive increase in secondary monoclinic CuO phase were also confirmed by X-ray diffraction study. Two types of grains and grain-boundaries were found in the microstructure. Such microstructure has great impact on the dielectric and electrical properties of CCTO samples. Experimental impedance data are being fitted with the equivalent electrical circuit models in accordance with the microstructure (discussed in section 3.5). Melted like phase appeared near the grain boundary region, which allowed a dense microstructure. The appearance of melted phase can be understood in terms of instability of copper in CCTO lattice [1,18–21] during the sintering at high temperature. Cu-ions are being separated from the lattice sites and move towards the surface layer

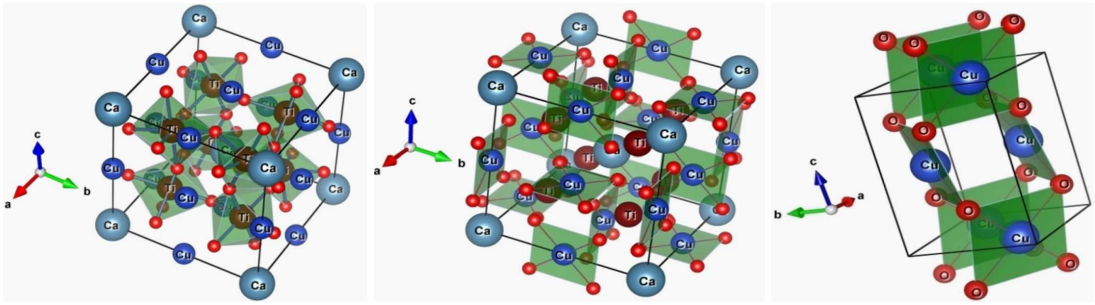

Figure 3. Refined structure with TiO_6 octahedra of CCTO3 (a), square planar coordination of oxygen around Cu in CCTO3 samples (b) and CuO monoclinic structure with square planar configuration of Cu–O bonds in CCTO3 samples

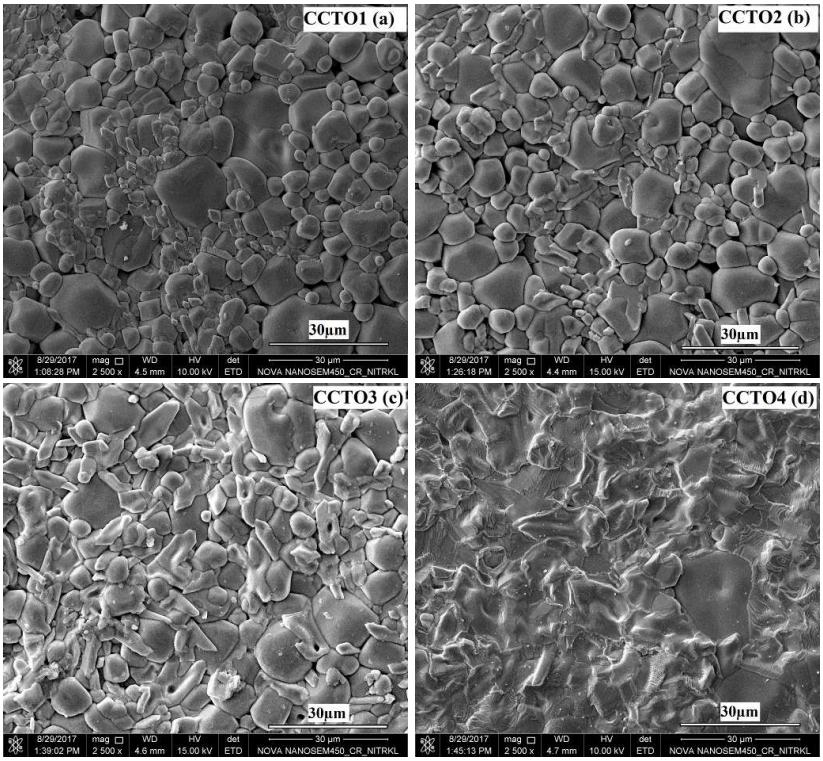

Figure 4. FESEM micrographs of: a) CCTO1, b) CCTO2, c) CCTO3 and d) CCTO4

due to thermal diffusion. These Cu-ions get oxidised and become CuO.

The amount of melted Cu-rich phase increases with the increase of sintering temperature, which can lead to an effective reduction in the grain boundary dimension. Generally, grain growth is inhibited in microwave processing of ceramics and therefore similar average grain size has been observed for all samples.

3.3. Dielectric study

Figure 5 shows the frequency dependent dielectric properties at room temperature. Dielectric constant (ε_r) increases with sintering temperature from 1000 to 1050 °C, but there is a certain drop in dielectric constant, when sintering temperature is 1075 °C. Opposite trend is observed for $\tan\delta$. Possible reasons behind the increase and decrease in ε_r values could be related to the sample microstructures. Improved dielectric properties of the CCTO samples with the increase of sintering temperature can be explained on the basis of the internal barrier layer capacitance model (IBLC). In IBLC, effective dielectric constant is proportional to the ratio of grain and grain-boundary thickness ($\varepsilon_{eff} \approx t_g/t_{gb}$, t_g is grain thickness and t_{gb} is grain-boundary thick-

Table 1. Elemental analysis data of distinct grains and melted phase of all samples

Samples	Distinct grain				Melted phase			
	Ca	Cu	Ti	O	Ca	Cu	Ti	O
CCTO1	6.21	15.27	26.66	51.86	0.35	47.84	2.75	49.05
CCTO2	6.16	15.29	27.22	51.34	0.29	64.68	2.75	32.28
CCTO3	6.34	15.23	25.35	53.08	0.68	71.31	3.33	24.69
CCTO4	6.09	14.94	23.94	55.04	0.31	59.56	1.83	38.30

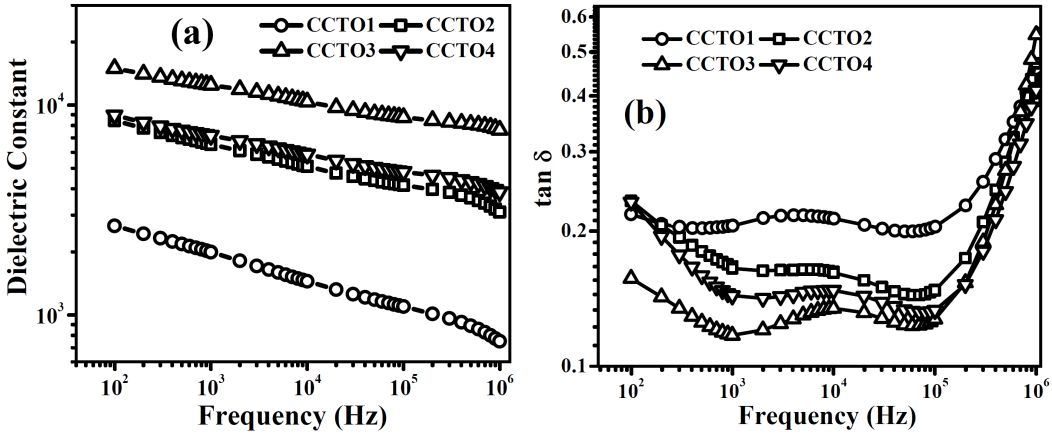

Figure 5. Frequency dependence of: a) dielectric constant (ε_r), b) tanδ at RT

ness). Here, average grain dimension remains almost unchanged and grain-boundary dimension is reduced due to the increase in melted phase near grain boundary regions. However, the sample CCTO4 shows lower ε_r value compared to the CCTO3, which can be attributed to non-stoichiometry of Cu content in CCTO lattice due to its volatile nature. Different amount of Cu-rich melted phase in different samples can significantly modify the impedance properties.

Variations of dielectric properties as a function of temperature (from RT to 300 °C) at four different frequencies (1, 10, 100 and 1000 kHz) have been illustrated in Figs. 6, 7, 8 and 9 for the samples CCTO1, CCTO2, CCTO3 and CCTO4, respectively. In our previous report [1], no dielectric anomalies were found within the measuring temperature range from RT to 150 °C. However, in this work, dielectric anomaly in the form of broad peaks is observed in temperature range between 125 to 300 °C for all samples. Those broad peaks appear to be shifted to higher temperature with increasing frequency. This relaxor-type behaviour may be attributed to the surface-layer-related Maxwell-Wagner relaxation

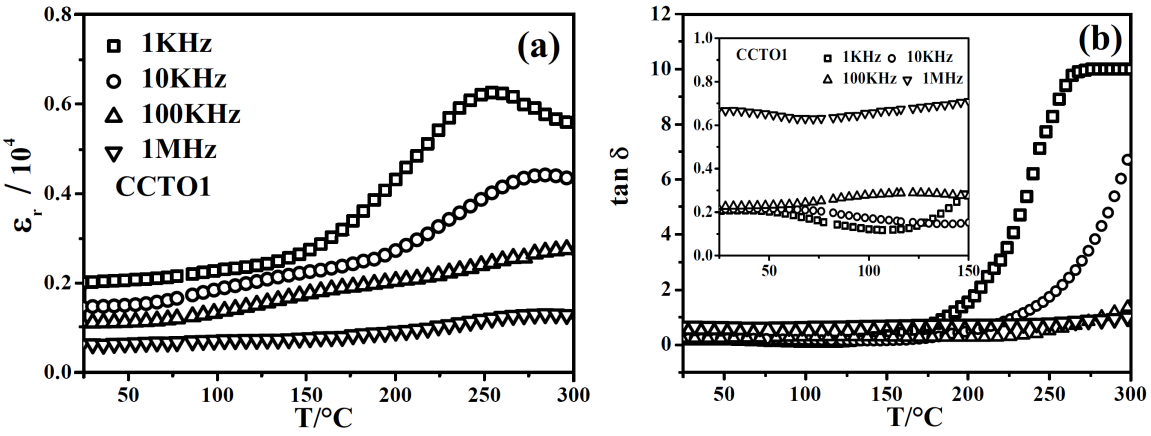

Figure 6. Temperature variation of: a) dielectric constant (ε_r) and b) tanδ at different frequencies of CCTO1

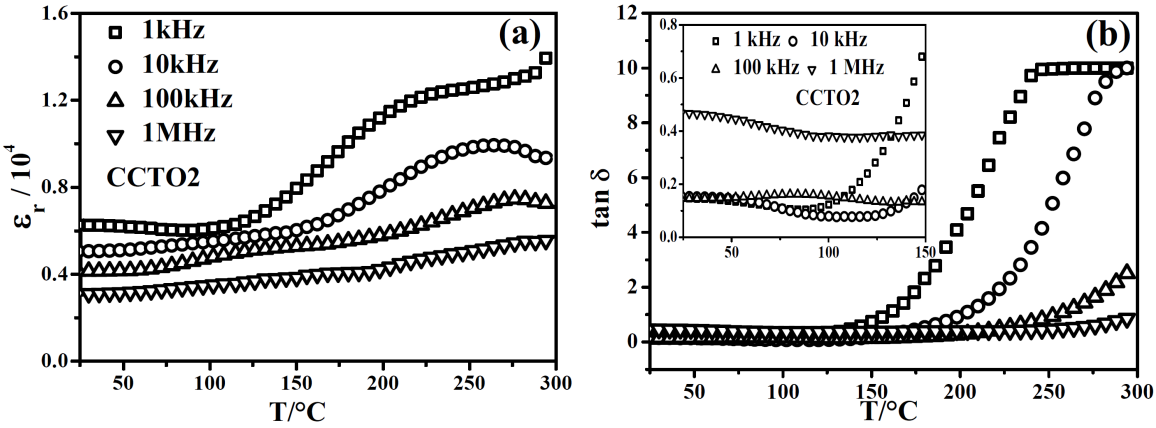

Figure 7. Temperature variation of: a) dielectric constant (ε_r) and b) tanδ at different frequencies of CCTO2

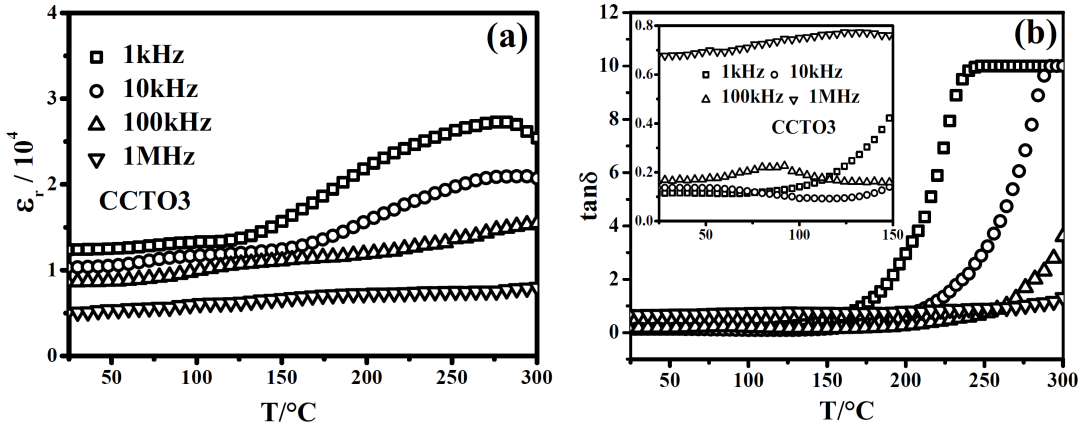

Figure 8. Temperature variation of: a) dielectric constant (ε_r) and b) tanδ at different frequencies of CCTO3

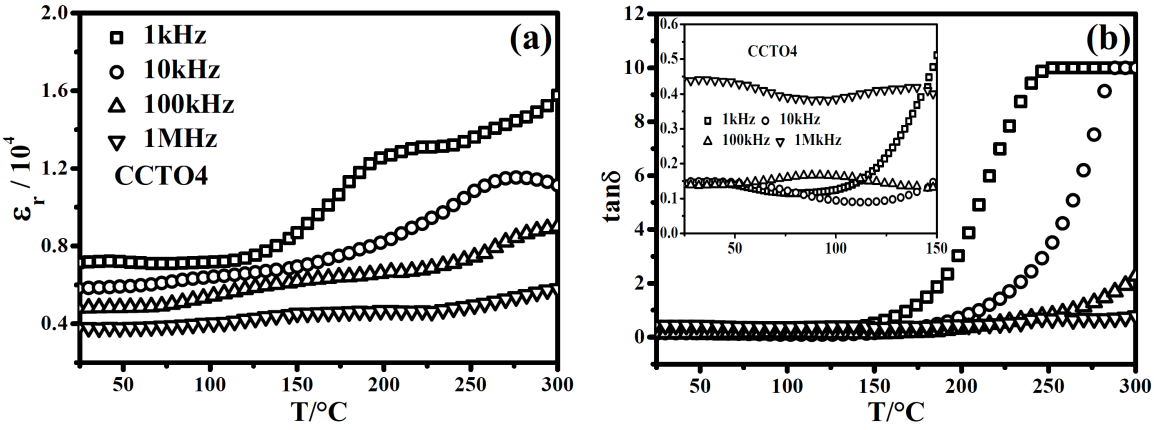

Figure 9. Temperature variation of: a) dielectric constant (ε_r) and b) tanδ at different frequencies of CCTO4

due to the inhomogeneous distribution of oxygen vacancies [22]. These broad peaks also exhibit the characteristics of a relaxor ferroelectric, which can be understood by a diffuse phase transition. The dielectric maximum interpreted a dynamic freezing or glass-like transition temperature. Such relaxor ferroelectric transition may also be attributed to "correlated off-centre displacement of Ti^{4+} ions along each single <001> column but without any correlation between neighboring columns" [23]. A sharp increase in tan δ value was found near 150 °C at 1 kHz for all samples. Above ≈ 150 °C, the temperature dependence of tan δ can be explained on the basis of piling up charges at the grain boundaries, because conduction mechanism is a thermally activated process [24].

3.4. Impedance study

Complex impedance spectroscopy (CIS) is one of the most powerful and non-destructive techniques, which can easily separate different sources contributing to electrical properties of material over a wide range of frequency and temperature. It is also useful to investigate the probable mechanisms, which account for the attractive dielectric properties of the CCTO ceramics. In polycrystalline ceramics, the total observed impedance mainly originated from three different parts of the materials: i) grains (bulk), ii) grain boundaries (GB) and iii) electrode-sample interface. An equivalent parallel *R-C* circuit can represent electrical response of each part, where R and C are resistance and capacitance. Sometimes equivalent circuit with constant phase element (*CPE* or *Q*) is better fitted with experimental data. Impedance of constant phase element can be represented as:

$$Z^*_{CPE} = \frac{1}{Y_0(j \cdot \omega)^n} \tag{2}$$

where Y_0 and n are constants. For ideal capacitor $Y_0 = C$ and $n = 1$, for ideal resistance $Y_0 = 1/R$ and $n = 0$. We have taken impedance data within the frequency window from 100 Hz to 1 MHz at an interval of 10 °C from room temperature to 300 °C following a heating rate of 2 °C/min. Complex impedance $Z^* = Z' - jZ''$ is made of real part, $Z' = |Z^*| \cos\phi$ and imaginary part, $-Z'' = |Z*| \sin\phi$, where ϕ is the phase. Figure 10 shows the behaviour of real part of impedance (Z') as a function of frequency at different temperatures for all four samples. Low frequency plateau is due to the long-range migration of charge carriers (DC conduction). After a certain frequency (called crossover frequency), dispersion started in Z' vs. frequency plot. The crossover frequency shifted to higher frequency region with increase in temperature. This kind of behaviour is an indication of hopping conduction of charge carriers. At high frequency, the merging nature may be due to the release of space charge to grain boundary because of decreas-

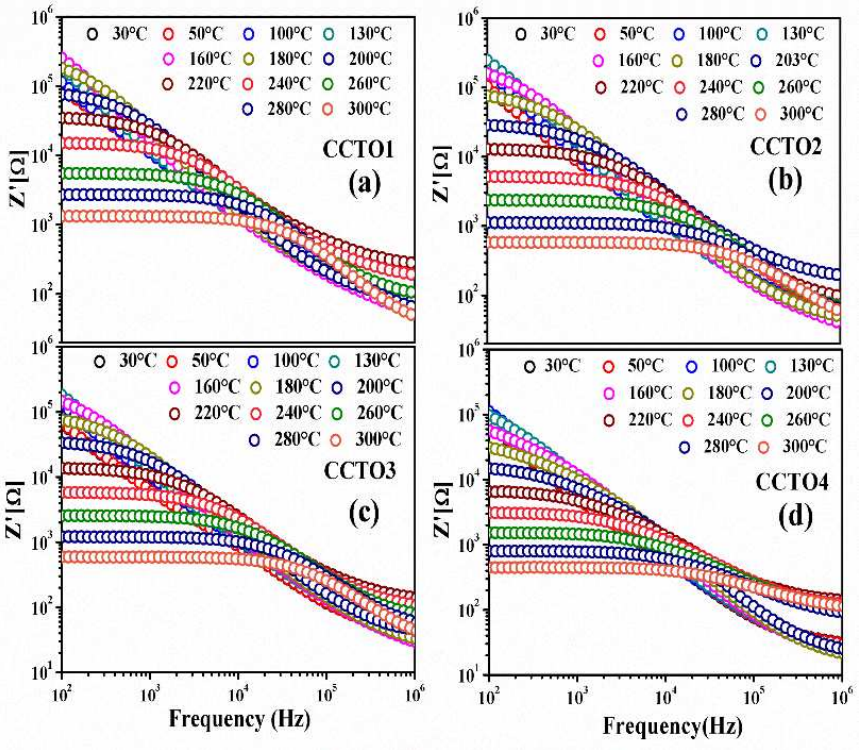

Figure 10. Z' as a function of frequency at different temperatures

ing barrier width [25]. At low frequency (~100 Hz) region, Z' is found to exhibit PTCR behaviour up to certain temperature and then suddenly follows the NTCR behaviour at high temperature. Such transitions from PTCR (positive temperature coefficient of resistance) to NTCR (negative temperature coefficient of resistance) occur at different temperature for different samples. For the CCTO1, it is ~160 °C and for the CCTO2, CCTO3 and CCTO4 it is ~130 °C. According to the Heywang-Jonkar model [26,27], a potential barrier is being developed due to the electron traps or acceptor states present in the grain boundary, where electrons are attracted by the traps coming from the grain. As a result, there must be the formation of electron depletion layer. As temperature increases, the energy of the trapped electrons as well as the potential barrier increases. Hence, the resistance increases. After reaching the threshold value (Fermi energy), the trapped electrons start jumping to conduction band and further increase in barrier width is prevented. Additional increase in temperature causes the barrier width to become narrower and the resistance decreases. Hence, at a certain temperature there is a transition from PTCR to NTCR behaviour. This anomalous nature may also be due to the electrical heterogeneity of the ceramics.

Figures 11 and 12 show the imaginary part of impedance (Z'') and its normalized value (Z''/Z''_{max}) as a function of frequency (f) at different temperatures for all samples, respectively. Nature of these plots includes: i) appearance of a peak after a certain temperature within the used frequency window, ii) shift of the peaks towards higher frequency zone with increasing temperature and iii) asymmetric peak broadening and decrease in the value of imaginary part of impedance with increasing temperature. This type of behaviour is signature of temperature dependent electrical relaxation phenomena, which was reported in several single crystals [28,29].

Asymmetric broadening of peaks conveys the presence of electrical processes with spread of the relaxation time [2]. Grain boundary relaxation occurred probably at high temperature. The most probable relaxation time can be represented by the relation $\tau = 1/(2\pi f_m)$, where f_m is the peak frequency at a particular temperature. The relaxation time (τ) relates the activation energy (E_a) and temperature (T) by the Arrhenius Equation: $\tau = \tau_0 \exp(E_a/KT)$. In this equation, τ_0 is the pre-exponential factor, which is the relaxation time at infinite temperature. The slope of $\ln(\tau)$ vs. $1000/T$ plot, which is a straight line (Fig. 13a) gives the activation energy $E_a(Z''_{exp})$. Activation energies, found from relaxation peaks of Z''_{exp}, are ~1.05, 1.00, 0.99 and 0.97 eV for the CCTO1, CCTO2, CCTO3, and CCTO4 ceramics, respectively. Corresponding theoretical relaxation times at infinite temperature (τ_0) for successive samples are $\sim 2.09 \times 10^{-15}$, 2.66×10^{-15}, 4.35×10^{-15} and 1.05×10^{-14} s, respectively. Relaxation parameters, E_a and τ_0, related to oxygen vacancies, are reported to be ~1.0 eV and 10^{-11} to 10^{-16} s, respectively [30,31], which suggests that the activation energy, extracted from Arrhenius plots in the present study, is associated with relaxation of oxygen vacancies.

Band gap is the energy difference between top of the valance band and bottom of the conduction band. Band

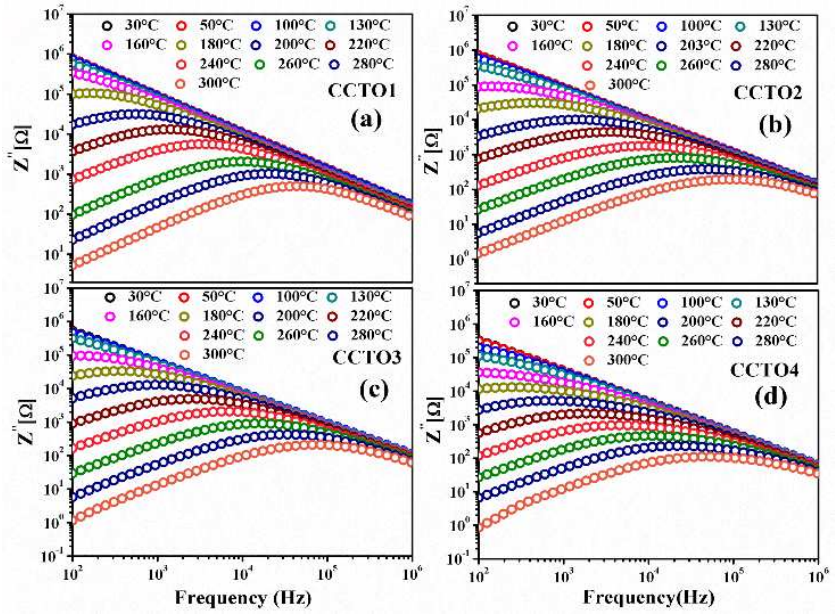

Figure 11. Z'' **as a function of frequency (**f**) at different temperatures**

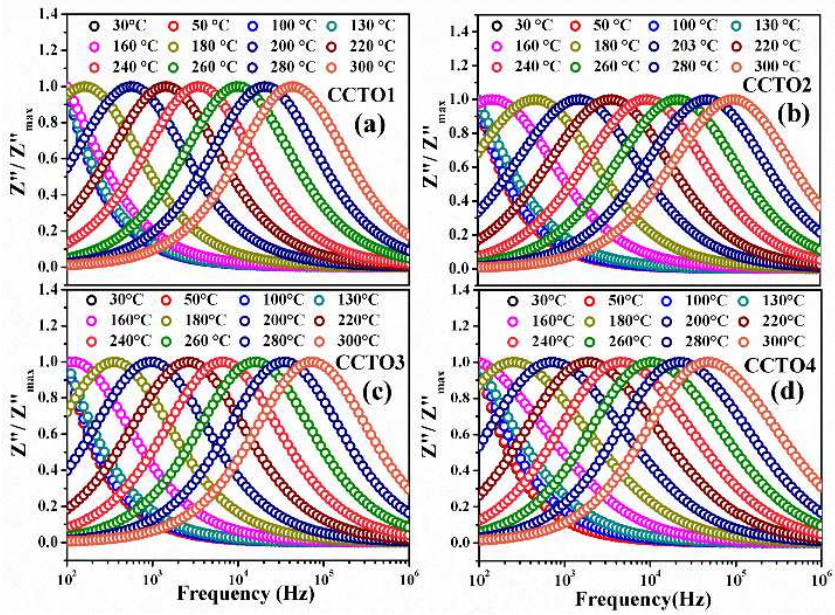

Figure 12. Z''/Z''_{max} **as a function of frequency (**f**) at different temperatures**

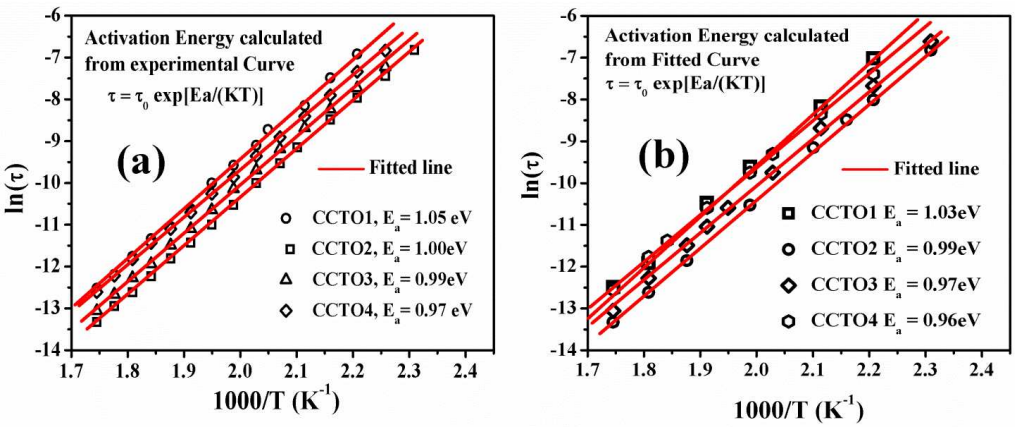

Figure 13. Activation energy estimated from: a) experimental $Z''(f,T)$ **data and b) fitted** $Z''(f,T)$ **data**

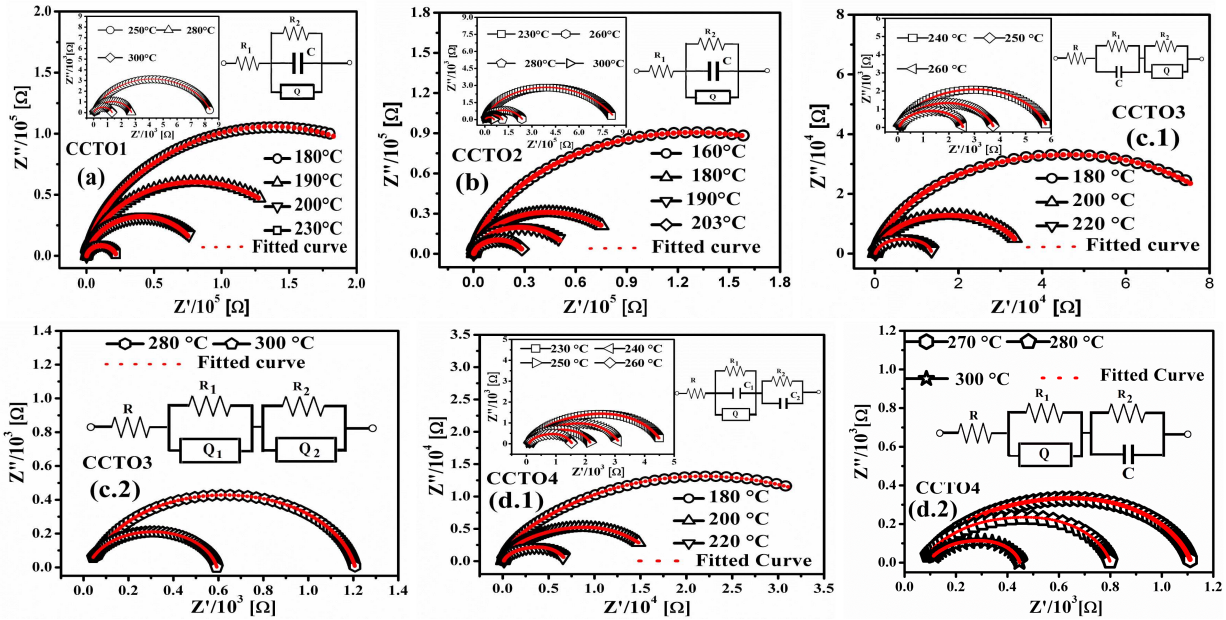

Figure 14. Cole-Cole plot and associated fitting for impedance data of: a) CCTO1 (180 to 300 °C), b) CCTO2 (160 to 300 °C), c.1) CCTO3 (180 to 260 °C), c.2) CCTO3 (280 to 300 °C), d.1) CCTO4 (180 to 260 °C) and d.2) CCTO4 (270 to 300 °C)

gap can be tuned by doping, hence creating the acceptor or donor states near valance and conduction bands, respectively. By using diffuse reflectance UV-Vis spectroscopy, Kushwaha *et al.* [45] reported the direct band gap of CCTO powder to be ~1.5 eV. This group has also reported that the higher energy absorption edge appears due to the direct transition from (Cu 3*d*)–(O 2*p*) hybridized valance band to the (Ti 3*d*) conduction band and the lower energy absorption is due to the transition between valance band and un-occupied (Cu 3*d*) band. Xiao *et al.* [46] reported that the border-line deep level of V_O^{2+} is at ~1.06 eV bellow the conduction band, while the values are ~0.53 eV and ~0.1 eV for V_O^{1+} and V_O, respectively. Therefore, in the present study we expect that the oxygen vacancies are mostly in effective 2+ charge states.

Figure 14 shows Z'' vs. Z' Cole-Cole plot for the sample CCTO1, CCTO2, CCTO3 and CCTO4. Single arc appeared with centre bellow the Z' axis. If Z' axis contains the centre of a semicircular arc, then the phenomenon is associated with the single relaxation time and known as Debye-type relaxation [32,33]. When the centres are below the real axis, there is distribution of the relaxation time known as non-Debye-type relaxation [34]. The non-zero intercept at high frequency region corresponds to grain response and low-frequency arc represents grain-boundary response [24]. We proposed equivalent circuit models to fit the experimental impedance data using ZSimpWin software (Version 3.21) and tried to connect the electrical response and the microstructure of the samples in the presence of Cu-rich melted (inter-granular) phase. The Z''/Z''_{max} vs. frequency plot is also fitted with respective circuit model (Fig. 15). Figure 13b shows the Arrhenius plot corresponding to fitted Z''/Z''_{max} vs. frequency data. Activation energies $E_a(Z''_{fitted})$ found from the fitted Z''/Z''_{max} vs. frequency data are 1.03, 0.99, 0.97 and 0.96 eV, respectively, which are close to the values of $E_a(Z''_{exp})$.

Sets of R, C and Q at different temperatures for different samples were also determined (they are not presented here). In the CCTO1 and CCTO2 samples, the amount of melted grain is small compared to that of the CCTO3 and CCTO4. Accordingly, this effect is reflected in the equivalent circuit models fitted to the respective Cole-Cole plots. In the samples CCTO1 and CCTO2, grain (represented by R) and grain boundary (parallel combination of R, C and Q) are the major contributors to the impedance profile. Electrical properties of such CCTO ceramics with nearly stoichiometric grains and Cu-rich melted phase maybe understood based on different interfaces like grain-grain interface, grain-melted phase interface etc.

In Fig. 16, we proposed a model to support the choice of electrical circuits. Microstructure of all samples includes two types of grains: i) distinct grain and ii) melted phase. Hence, there must be two types of interfaces: i) grain-grain interface and ii) grain-melted phase interface. This model suggests two approaches:

i. Grain and melted phase have comparable or average properties but the interfaces of two grains or grain-melted phase may be different in nature
ii. Grain and melted phase have different properties but two types of above said interfaces show comparable properties.

On the other hand, in the CCTO3 and CCTO4 samples, three contributions appeared in equivalent electrical circuit. In the CCTO3 and CCTO4 samples, electrical circuits also changed after a certain temperature (about 260 °C), whereas some pure ideal capacitance (C) behaviour transformed into non-ideal capacitance

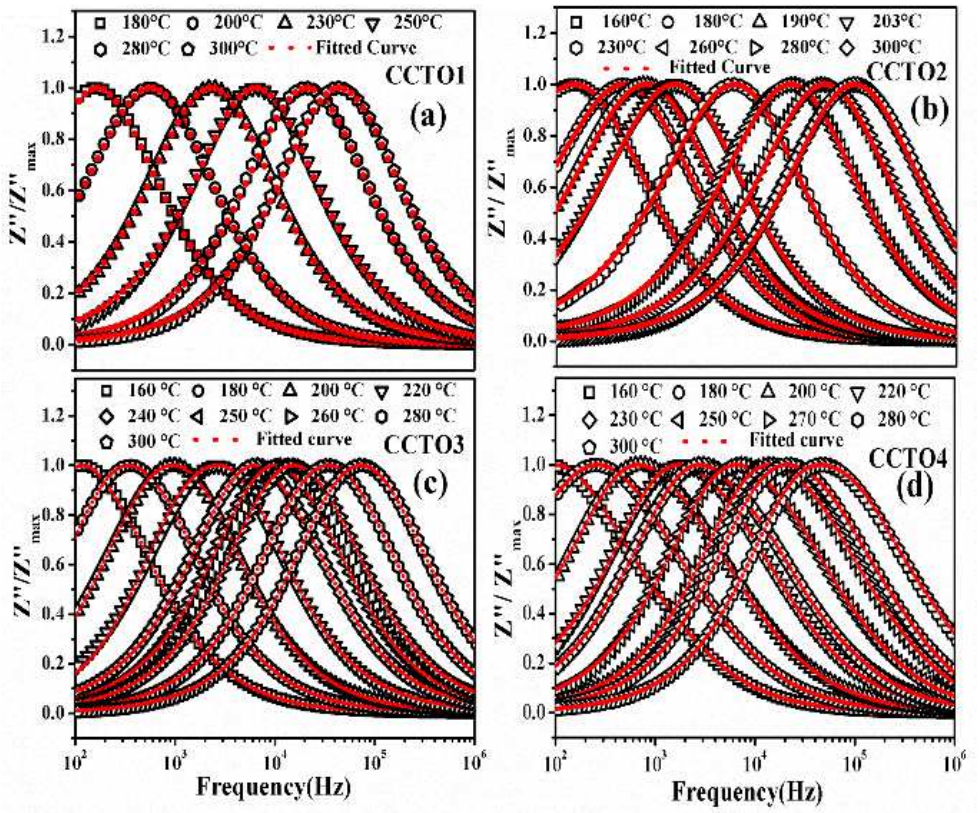

Figure 15. Fitted Z''/Z''_{max} as a function of frequency (f) at different temperatures

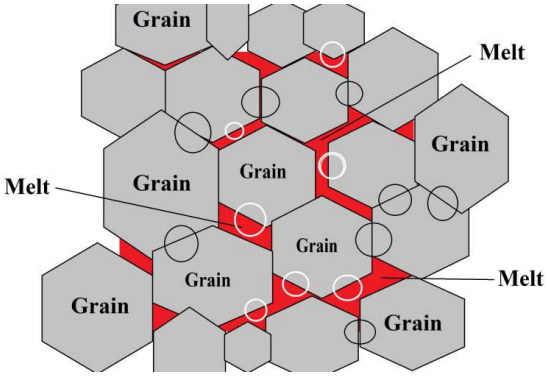

Figure 16. Schematic representation of grain, melted phase and different interfaces (white circles mark interface between grain and melted phase, black circles show interfaces between two grains)

or constant phase element (Q) behaviour. These results suggest that grain boundary properties are temperature dependent. It is also evident that after a certain amount of melted phase (which is a function of sintering temperature), degree of heterogeneity increases and moderate amount of CuO phase is required to get best dielectric properties.

Modulus formalism helps us to understand the type of polarization and electrical transport mechanism more clearly. An electric modulus (M^*) can be defined in terms of reciprocal of the complex dielectric permittivity:

$$\varepsilon^* = \frac{1}{j\omega C_0 Z^*} \tag{3}$$

as

$$M^* = \frac{1}{\varepsilon^*} = M' + jM'''' = j\omega C_0 Z^* = j\omega C_0 (Z' - jZ'') = \\ = \omega C_0 Z'' + j\omega C_0 Z' \tag{4}$$

So, the real part of modulus is $M' = \omega C_0 Z''$ and the imaginary part is $M'' = \omega C_0 Z'$.

Electrical response may be due to the delocalized long-range conduction or localized dipole relaxation [35]. However, both localized and delocalized conductions are found in bulk materials and therefore produce same geometrical capacitance [35]. Utilization of the imaginary part of the impedance (Z'') is significant for resistive and/or conductive analysis when the long-range conductivity is concerned. At the same time, the imaginary part of electrical modulus (M'') is relevant where localized dipole relaxation is dominating mechanism [35,36]. Figure 17 shows the variation of the real part of modulus as a function of frequency at different temperatures. Value of M' is low at low frequency and increases asymptotically with frequency for different temperatures. If the magnitude of M' at different temperatures tends to zero, and coincide each other in the low-frequency region, then there will be negligibly small contribution of electrode effect [33,37–39]. However, bellow 170 °C and at low frequency, the M' values are non-zero. Therefore, significant electrode contribution may be present. Value of M' increases with the increase of frequency and might be reaching the limiting

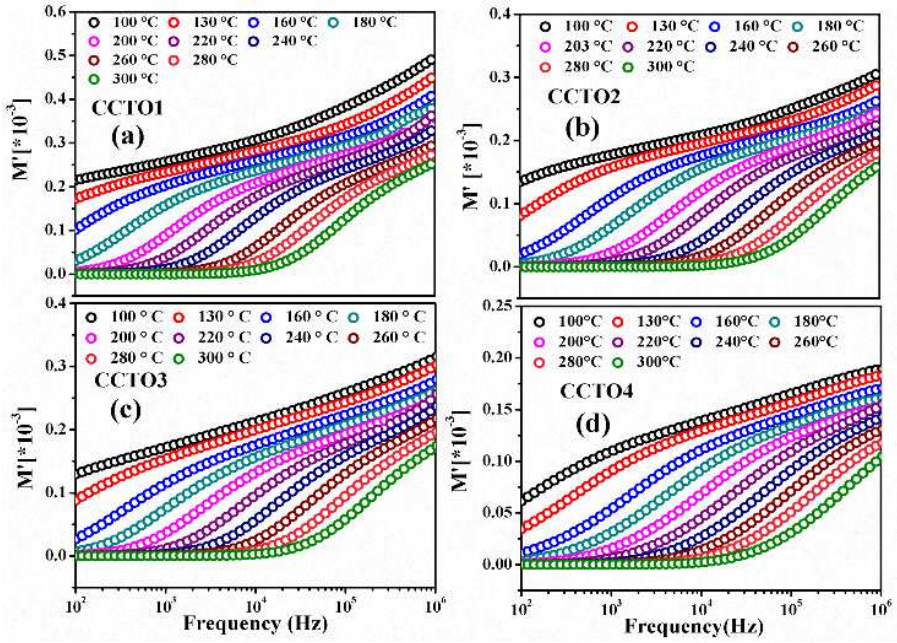

Figure 17. Real part of electrical modulus as a function of frequency at different temperatures for: a) CCTO1, b) CCTO2, c) CCTO3 and d) CCTO4

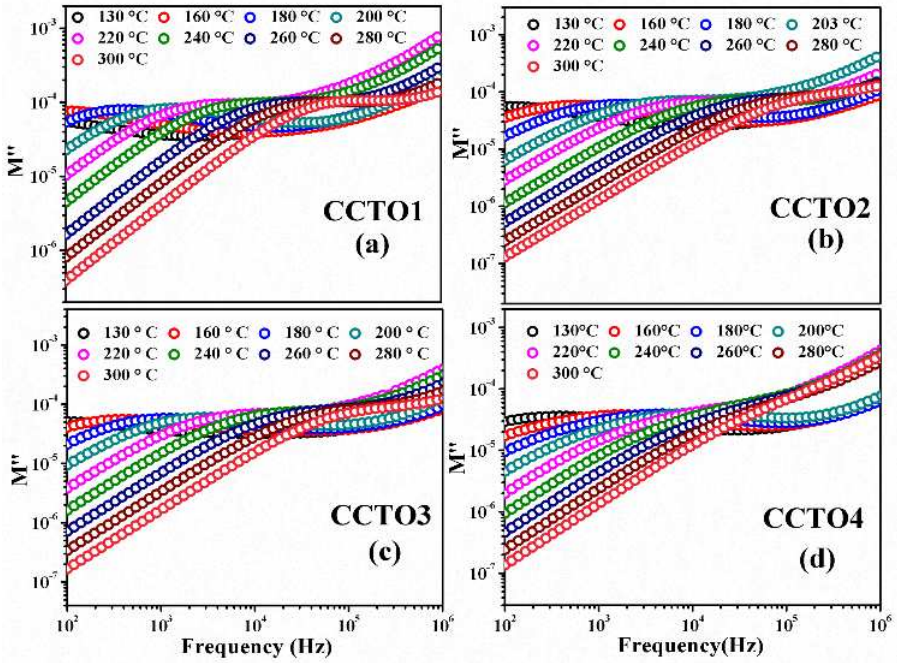

Figure 18. Imaginary part of electrical modulus as a function of frequency at different temperatures for: a) CCTO1, b) CCTO2, c) CCTO3 and d) CCTO4

value (M_∞) at higher frequencies, which may be beyond the frequency domain of experimental measurement set-up. This observation may be due to the lack of restoring force governing the mobility of charge carriers under the action of an induced electric field [24,38–41]. Increase in M' value with increasing frequency may be attributed to the relaxation phenomena associated with short range mobility of the charge carriers, which is spread over a range of frequencies [39].

In the imaginary part of electrical modulus $M''(f,T)$ spectra, frequency region below the peak maxima is associated with the long-range mobility and above the peak maxima, short-range mobility of charge carriers dominates [24,42]. The region where the peak appears in $M''(\omega)$ suggests a transition from long-range to short-range mobility of charge carriers. Figure 18 shows the variation of M'' as a function of frequency at different temperatures. Figure 19 shows the Arrhenius plot corresponding to peak frequencies of M''/M''_{max} vs. frequency data and calculated $E_a(M'')$ for CCTO1, CCTO2, CCTO3 and CCTO4 are 1.04, 1.01, 1.0 and 0.97 eV, respectively. The values of activation energies

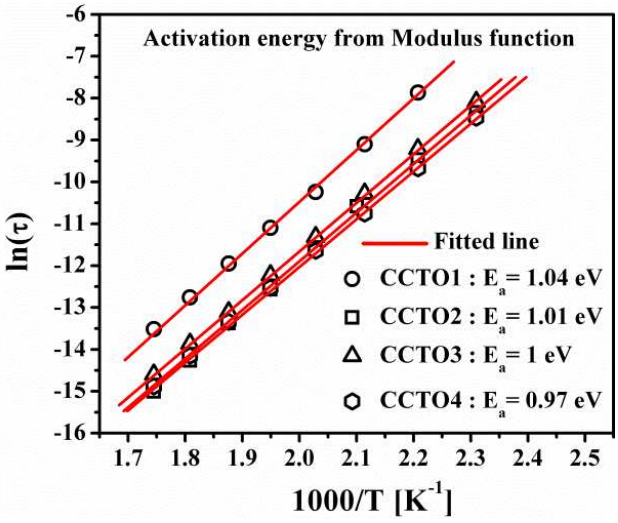

Figure 19. Activation energy calculated from the imaginary part of electrical modulus

are in close agreement with $E_a(Z''_{exp})$ and $E_a(Z''_{fitted})$. In M''/M''_{max} and Z''/Z''_{max} plots as functions of frequency plotted in the same graph (Fig. 20), mismatch appeared between two peaks. Such behaviour is attributed to non-ideal Debye-like and short-range movement of charge carriers [38–41]. If the peaks overlap each other, the behaviour is ideal Debye-like and associated with long-range movement of charge carriers [38–41]. As both short-range and long-range movement of charge carriers are present in the samples, hopping mechanism in the presence of different defect states are very important and these defects play significant role in modifying the dielectric properties. High temperature firing of the ceramics causes creation of oxygen vacancies in grains. As a result, grains become n-type semiconducting in nature. Each of the oxygen vacancies corresponds to two electrons in the lattice. A Ti^{4+} ion usually captures one of them and reduction process occurs from Ti^{4+} to Ti^{3+}. Ti^{3+} and oxygen vacancies as a whole formed a defect dipole cluster, which may cause effective enhancement of dielectric constant and reduction of loss.

In order to confirm the poly dispersive nature of the dielectric relaxation and its temperature dependence, Z'' is plotted in scaled co-ordinates, i.e. Z''/Z''_{max} vs. f/f_{max}. If all the impedance profiles collapse into one master curve, it implies that the distribution of the relaxation times is independent of temperature [24,37,40,43,44], which is shown in Fig. 21.

IV. Conclusions

Polycrystalline $CaCu_3Ti_4O_{12}$ (CCTO) ceramics was synthesized by microwave assisted solid-state reaction. Different sintering temperatures were used, i.e. 100, 1025, 1050 and 1075 °C (samples CCTO-1, CCTO2, CCTO-3 and CCTO-4 respectively). All sintered pellets show diffraction pattern of the cubic perovskite phase with space group $Im\bar{3}$ along with several peaks of the secondary phase identified as CuO.

For CCTO3, maximum dielectric constant (at room temperature) found at ≈15000 with $\tan\delta \approx 0.15$ at 100 Hz. Therefore, proper amount of secondary phase plays important role behind the improvement in dielectric properties. In the CCTO1 and CCTO2 samples, Cu-rich melted phase content was low. Impedance study confirmed the contribution of grain and grain boundary to electrical properties. However, in the CCTO3 and CCTO4 samples, Cu-rich melted phase was comparatively large; hence, the impedance data were fitted with three contributions (two different type grains

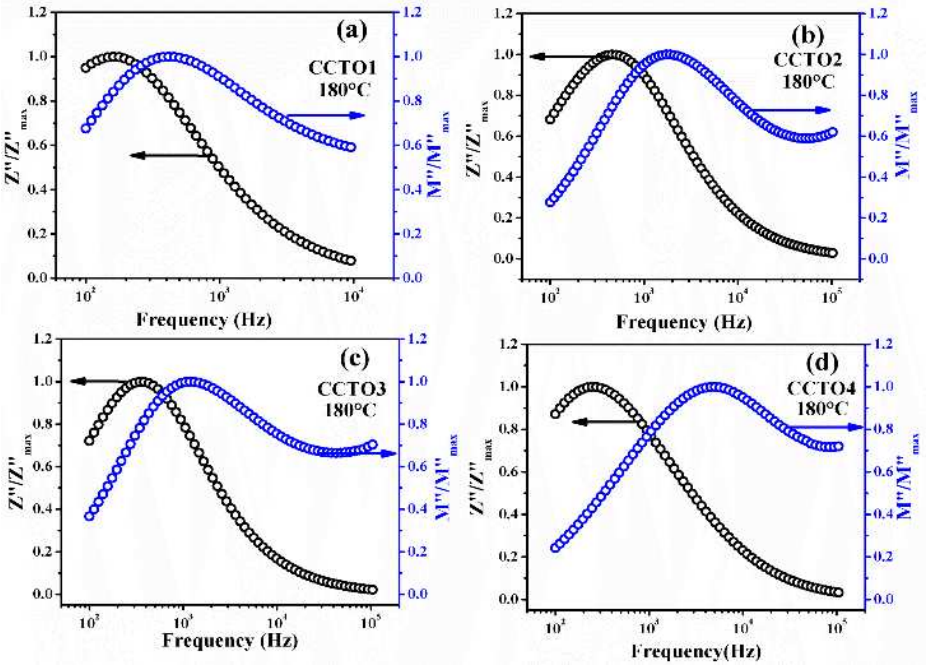

Figure 20. Frequency dependence of Z''/Z''_{max} and M''/M''_{max} in same graph for: a) CCTO1, b) CCTO2, c) CCTO3 and d) CCTO4 all at 180 °C

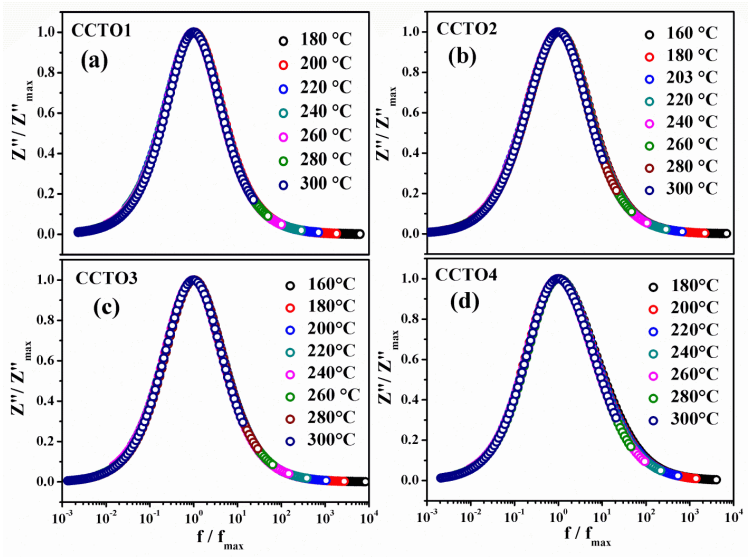

Figure 21. Scaling behaviour of Z'' at different temperatures for: a) CCTO1, b) CCTO2, c) CCTO3 and d) CCTO4

and grain-boundary). Activation energy calculated from three different sources Z''_{exp}, Z''_{fitted} and M''_{exp} are in close agreement. This behaviour indicates the involvement of the same kind of charge carrier in different relaxation phenomena. Both long and short-range migration of charge carriers is responsible for the overall electrical behaviour of the samples. Modulus analysis explained the presence of hopping mechanism in electrical transport processes. Mismatch between the peaks of Z''/Z''_{max} and M''/M''_{max} suggests towards a dominating short-range movement of charge carriers (localized conduction) in the CCTO ceramics. Electrical behaviour clearly indicates the deviations from the ideal Debye nature. There is a spread of relaxation time for non-Debye nature and the most probable relaxation time gives the activation energy. Z''/Z''_{max} vs. f/f_{max} plot suggested the temperature independent nature of most probable relaxation time for all samples.

The amount of CuO phase is a function of sintering temperature. The presence of moderate amount of Cu-rich phase can achieve best dielectric properties. Large amount of CuO phase can cause non-stoichiometry or deficiency in the CCTO structure, which debase the dielectric properties.

Acknowledgement: The authors acknowledge the financial support of DRDO (Government of India) [Project No. ERIP/ER/1406037/M/01/1558. We would like to thank Prof. Santosh Kumar Sahoo of department of Metallurgy and Materials Engineering [NIT Rourkela, Odisha, 769008] for measurement at X-ray Diffraction Lab (With Texture Cradle)].

References

1. B. Samanta, P. Kumar, C. Prakash, "Effect of sintering temperature and Cu-rich secondary phase on dielectric properties of microwave processed $CaCu_3Ti_4O_{12}$ ceramics", *Ferroelectrics*, **517** [1] (2017) 46–57.
2. A. Sen, U.N. Maiti, R. Thapa, K.K. Chattopadhyay, "Temperature-dependent ac conductivity and dielectric response of vanadium doped $CaCu_3Ti_4O_{12}$ ceramic", *Appl. Phys. A*, **104** [4] (2011) 1105–1111.
3. A.P. Ramirez, M.A. Subramanian, M. Gardel, G. Blumberg, D. Li, T. Vogt, S.M. Shapiro, "Giant dielectric constant response in a copper-titanate", *Solid State Commun.*, **115** [5] (2000) 217–220.
4. D. Chakravarty, P. Singh, S. Singh, "Electrical conduction behavior of high dielectric constant perovskite oxide $La_xCa_{1-3x/2}Cu_3Ti_4O_{12}$", *J. Alloys Compd.*, **438** [1-2] (2007) 253–257.
5. M. Li, Z. Shen, M. Nygren, A. Feteira, D. C. Sinclair, A. R. West, "Origin(s) of the apparent high permittivity in $CaCu_3Ti_4O_{12}$ ceramics: clarification on the contributions from internal barrier layer capacitor and sample-electrode contact effects", *J. Appl. Phys.*, **106** [10] (2009) 104106.
6. M.C. Ferrarelli, D.C. Sinclair, A.R. West, H.A. Dabkowska, A. Dabkowski, G.M. Luke, "Comment on the origin(s) of the giant permittivity effect in $CaCu_3Ti_4O_{12}$ single crystals and ceramics", *J. Mater. Chem.*, **19** [33] (2009) 5916–5919.
7. D.C. Sinclair, T.B. Adams, F.D. Morrison, A.R. West, "$CaCu_3Ti_4O_{12}$: One-step internal barrier layer capacitor", *Appl. Phys. Lett.*, **80** [12] (2002) 2153–2155.
8. T.B. Adams, D.C. Sinclair, A.R. West, "Characterization of grain boundary impedances in fine- and coarse-grained $CaCu_3Ti_4O_{12}$ ceramics", *Phys. Rev. B*, **73** (2006) 094124.
9. L. Liu, H. Fan, P. Fang, X. Chen, "Sol-gel derived $CaCu_3Ti_4O_{12}$ ceramics: Synthesis, characterization and electrical properties", *Mater. Res. Bull.*, **43** [7] (2008) 1800–1807.
10. M. Mohamad, Ahmad, K. Yamada, "Grain size effect on the giant dielectric constant of $CaCu_3Ti_4O_{12}$ nano-ceramics prepared by mechano-synthesis and spark plasma sintering", *J. Appl. Phys.*, **115** [15] (2014) 154103.
11. J. Liu, R.W. Smith, W.N. Mei, "Synthesis of the giant dielectric constant material $CaCu_3Ti_4O_{12}$ by wet-chemistry methods", *Chem. Mater.*, **19** [24] (2007) 6020–6024.
12. P. Lunkenheimer, R. Ficht, S.G. Ebbinghaus, A. Loidl, "Nonintrinsic origin of the colossal dielectric constants in $CaCu_3Ti_4O_{12}$", *Phys. Rev. B*, **70** (2004) 172102.

13. I. Burn, *Engineered Materials Handbook Volume 4: Ceramics and Glasses*, ASM International. The Materials Information Society, 1991.
14. E.J.J. Mallmann, M.A.S. Silva, A.S.B. Sombra, M.A. Botelho, S.E. Mazzetto, A.S. De menezes, A.F.L. Almeida, P.B.A. Fechine, "Dielectric properties of $Ca_{0.7}Bi_{0.3}Ti_{0.7}Cr_{0.3}O_3$ (CBTC) - $CaCu_3Ti_4O_{12}$ (CCTO) composite", *J. Elec. Mater.*, **44** [1] (2015) 295–302.
15. A.J. Moulson, J.M. Herbert, *Electroceramics: Materials, Properties, Applications*, Chichester, Wiley, 2003.
16. R. Schmidt, S. Pandey, P. Fiorenza, D.C. Sinclair, "Non-stoichiometry in "$CaCu_3Ti_4O_{12}$ (CCTO) ceramics", *RSC Advances.*, **3** [34] (2013) 14580–14589.
17. E.J. Abram, D.C. Sinclair, A.R. West, "A strategy for analysis and modelling of impedance spectroscopy data of electroceramics: Doped lanthanum gallate", *J. Electroceram.*, **10** [3] (2003) 165–177.
18. W.X. Yuan, Z. Luo, C. Wang, "Investigation on effects of CuO secondary phase on dielectric properties of $CaCu_3Ti_4O_{12}$ ceramics", *J. Alloys Comp.*, **562** (2013) 1–4.
19. W.X. Yuan, "Investigation on the decomposable process and the secondary liquid phase effect on the dielectric properties of $CaCu_3Ti_4O_{12}$ ceramics", *J. Phys. D: Appl. Phys.*, **42** [17] (2009) 175401.
20. H.J. Liang, L.F. Chao, H. Jun, L.Y. Hua, "Cu segregation and its effects on the electrical properties of calcium copper titanate", *Sci. China Technol. Sci.*, **54** [9] (2011) 2506–2510.
21. R. Lohnert, R. Schmidt, J. Topfer, "Effect of sintering conditions on microstructure and dielectric properties of $CaCu_3Ti_4O_{12}$ (CCTO) ceramics", *J. Electroceram.*, **34** [4] (2015) 241–248.
22. M.N. Zhang, K.B. Xu, G.J. Wang, C.C. Wang, "Dielectric anomalies in $CaCu_3Ti_4O_{12}$ at high temperatures", *Chinese Sci. Bull.*, **58** [7] (2013) 713–716.
23. S. Ke, H. Huang, H. Fan, "Relaxor behavior in $CaCu_3Ti_4O_{12}$ ceramics", *Appl. Phys. Lett.*, **89** [18] (2006) 182904.
24. A.K. Thomas, K. Abraham, J. Thomas, K.V. Saban, "Electrical and dielectric behavior of $Na_{0.5}La_{0.25}Sm_{0.25}Cu_3Ti_4O_{12}$ ceramics investigated by impedance and modulus spectroscopy", *J. Asian Ceram. Soc.*, **5** [1] (2017) 56–61.
25. B. Behera, P. Nayaka, R.N.P. Choudhary, "Impedance spectroscopy study of $NaBa_2V_5O_{15}$ ceramic", *J. Alloys Compd.*, **436** [1-2] (2007) 226–232.
26. W. Heywang, "Semiconducting barium titanate", *J. Mater. Sci.*, **6** [9] (1971) 1214–1224.
27. G.H. Jonker, "Some aspects of semiconducting barium titanate", *Solid State Electron.*, **7** [12] (1964) 895–903.
28. S. Lanfredi, J.F. Carvalho, A.C. Hernandes, "Electric and dielectric properties of $Bi_{12}TiO_{20}$ single crystals", *J. Appl. Phys.*, **88** [1] (2000) 283–287.
29. A.R. James, S. Priya, K. Uchino, K. Srinivas, "Dielectric spectroscopy of $Pb(Mg_{1/3}Nb_{2/3})O_3$-$PbTiO_3$ single crystals", *J. Appl. Phys.*, **90** [7] (2001) 3504–3508.
30. H.S. Shulman, D. Dragan, N. Setter, "Niobium doping and dielectric anomalies in bismuth titanate", *J. Am. Ceram. Soc.*, **83** [3] (2000) 528–532.
31. D. Li, X.P. Wang, Q.F. Fang, "Phase transition associated with the variation of oxygen vacancy/ion distribution in the oxide-ion conductor $La_2Mo_{2-x}W_xO_9$". *Phys. Status Solidi A*, **204** [7] (2007) 2270–2278.
32. Y-C. Lee, C-S. Chiang, Y-L. Huang, "Microwave dielectric properties and microstructures of Nb_2O_5-$Zn_{0.95}Mg_{0.05}TiO_3$ + $0.25TiO_2$ ceramics with Bi_2O_3 addition", *J. Eur. Ceram. Soc.*, **30** [4] (2010) 963–970.
33. M.B. Hossen, A.K.M.A. Hossain, "Complex impedance and electric modulus studies of magnetic ceramic $Ni_{0.27}Cu_{0.10}Zn_{0.63}Fe_2O_4$", *J. Adv. Ceram.*, **4** [3] (2015) 217–225.
34. P.R. Das, S. Behera, R. Padhee, P. Nayak, R.N.P. Choudhary, "Dielectric and electrical properties of $Na_2Pb_2La_2W_2Ti_4Ta_4O_{30}$ electro ceramics", *J. Adv. Ceram.*, **1** [3] (2012) 232–240.
35. D.K. Pradhan, R.N.P. Choudhary, C. Rinaldi, R.S. Katiyar, "Effect of Mn substitution on electrical and magnetic properties of $Bi_{0.9}La_{0.1}FeO_3$", *J. Appl. Phys.*, **106** (2009) 024102.
36. O. Raymond, R. Font, N. Suárez-Almodovar, J. Portelles, J.M. Siqueiros, "Frequency-temperature response of ferroelectromagnetic $Pb(Fe_{1/2}Nb_{1/2})O_3$ ceramics obtained by different precursors. Part II. Impedance spectroscopy characterization", *J. Appl. Phys.*, **97** (2005) 084108.
37. B.V.R Chowdari, R. Gopalakrishnan, "AC conductivity analysis of glassy silver iodomolybdate system", *Solid State Ionics*, **23** [3] (1987) 225–233.
38. K.P. Padmasree, D.K. Kanchan, A.R. Kulkarni, "Impedance and modulus studies of the solid electrolyte system 20 CdI_2–80 [xAg_2O–$y(0.7V_2O_5$-$0.3B_2O_3)$], where $1 \leq x/y \leq 3$", *Solid State Ionics*, **177** [5-6] (2006) 475–482.
39. M.A.L. Nobre, S. Lanfredi, "Grain boundary electric characterization of $Zn_7Sb_2O_{12}$ semiconducting ceramic: A negative temperature coefficient thermistor", *J. Appl. Phys.*, **93** [9] (2003) 5576–5582.
40. Md. K. Shamim, S. Sharma, S. Sinha, E. Nasreen, "Dielectric relaxation and modulus spectroscopy analysis of $(Na_{0.47}K_{0.47}Li_{0.06})NbO_3$ ceramics", *J. Adv. Dielec.*, **7** [3] (2017) 1750020.
41. S. Thakur, R. Rai, I. Bdikin, M.A. Valente, "Impedance and modulus spectroscopy characterization of Tb modified $Bi_{0.8}A_{0.1}Pb_{0.1}Fe_{0.9}Ti_{0.1}O_3$ ceramics", *Mater. Res.*, **19** [1] (2016) 1–8.
42. A. Shukla, R.N.P. Choudhary, A.K. Thakur, "Thermal, structural and complex impedance analysis of Mn^{4+} modified $BaTiO_3$ electroceramic", *J. Phys. Chem. Solids*, **70** [11] (2009) 1401–1407.
43. R. Tang, C. Jiang, W. Qian, J. Jian, X. Zhang, H. Wang, H. Yang, "Dielectric relaxation, resonance and scaling behaviors in $Sr_3Co_2Fe_{24}O_{41}$ hexaferrite", *Sci. Reports*, **5** (2015) 13645.
44. Q. Ke, X. Lou, Y. Wang, J. Wang, "Oxygen-vacancy-related relaxation and scaling behaviors of $Bi_{0.9}La_{0.1}Fe_{0.98}Mg_{0.02}O_3$ ferroelectric thin films", *Phys. Rev. B*, **82** (2010) 024102.
45. H.S. Kushwaha1, N.A. Madhar, B. Ilahi, P. Thomas, A. Halder, R. Vaish, "Efficient solar energy conversion using $CaCu_3Ti_4O_{12}$ photo-anode for photo catalysis and photoelectrocatalysis", *Sci. Reports*, **6** (2016) 18557.
46. H.B. Xiao, C.P. Yang, C. Huang, L.F. Xu, D.W. Shi, V.V. Marchenkov, I.V. Medvedeva, K. Barner, "Influence of oxygen vacancy on the electronic structure of $CaCu_3Ti_4O_{12}$ and its deep-level vacancy trap states by first-principle calculation", *J. Appl. Phys.*, **111** [6] (2012) 063713.